Input impedance and peripheral inhomogeneity of dog lungs

Z. HANTOS, B. DARÓCZY, B. SUKI, S. NAGY, AND J. J. FREDBERG
Kalmár Laboratory, József Attila University, and Institute of Experimental Surgery, Szent-Györgyi Medical University, H-6720 Szeged, Hungary; and Department of Environmental Science and Physiology, Harvard School of Public Health, and The Biomechanics Institute, Boston, Massachusetts 02215

HANTOS, Z., B. DARÓCZY, B. SUKI, S. NAGY, AND J. J. FREDBERG. *Input impedance and peripheral inhomogeneity of dog lungs.* J. Appl. Physiol. 72(1): 168–178, 1992.—Tracheal pressure, central airflow, and alveolar capsule pressures in cardiac lobes were measured in open-chest dogs during 0.1- to 20-Hz pseudorandom forced oscillations applied at the airway opening. In the interval 0.1–4.15 Hz, the input impedance data were fitted by four-parameter models including frequency-independent airway resistance and inertance and tissue parts featuring a marked negative frequency dependence of resistance and a slight elevation of elastance with frequency. The models gave good fits both in the control state and during histamine infusion. At the same time, the regional transfer impedances (alveolar pressure-to-central airflow ratios) showed intralobar and interlobar variabilities of similar degrees, which increased with frequency and were exaggerated during histamine infusion. Results of simulation studies based on a lung model consisting of a central airway and a number of peripheral units with airway and tissue parameters that were given independent wide distributions were in agreement with the experimental findings and showed that even an extremely inhomogeneous lung structure can produce virtually homogeneous mechanical behavior at the input.

pulmonary impedance; tissue impedance; alveolar pressures; forced oscillations; histamine infusion

IN A PREVIOUS STUDY (9), we have shown that the input impedance (Z_L) data obtained in normal dog lungs at low oscillation frequencies (0.125–4 Hz) are highly consistent with a four-parameter description. This model contained an airway compartment with frequency-independent resistance and inertance and a tissue compartment characterized by a real part inversely proportional to frequency and an elastance increasing linearly with the logarithm of frequency (13). Although analysis of the fitting performance of this model did not reveal any systematic error, the model-predicted partitioning of Z_L into airway (Zaw) and tissue (Zti) impedances was not validated. In other words, the questions of whether (*1*) all Newtonian resistances are located in the airway compartment and (*2*) how far a lumped representation of the lung periphery is justified in view of the evidence regarding the regional variability of alveolar pressure (P_A) even in the healthy lung (1–3, 6, 7, 15, 16, 18, 20–24) could not be addressed on the basis of the measured input quantities alone.

The aim of the present study was therefore to examine whether the model-predicted separation of Zaw and Zti is confirmed by measurements of local P_A values with the alveolar capsule technique (7). It will be shown that P_A exhibits a significant inhomogeneity, especially in the bronchoconstricted state, whereas Z_L remains consistent with the one-compartment lung periphery. This paradox can be resolved on the basis of a simulation model in which a number of largely different peripheral units share a common pathway.

METHODS

Animal preparation. Six mongrel dogs weighing 17.5–20.1 kg were studied in the supine position. They were anesthetized with pentobarbital sodium (initial dose of 30 mg/kg, supplemented hourly with 10-mg/kg doses). Systemic blood pressure was monitored in a catheter inserted into a femoral artery. Tracheotomy was performed, and a wide-bore (15–17 mm ID) thin-walled metal tube was fitted into the trachea. The animals were mechanically ventilated with a Harvard respirator at a tidal volume of 30 ml/kg and at frequencies of 10–15/min. A positive end-expiratory pressure was maintained at 5 cmH_2O. Paralysis was accomplished with pipecuronium bromide (0.1-mg/kg initial dose, supplemented with 0.05 mg/kg after 2 h), bilateral incisions were then made between the fifth and sixth ribs, and the sternum was split and widely retracted.

Pressure and flow measurements. Local alveolar pressures (P_{A_i}) were measured with a method similar to that described by Fredberg et al. (6). Light Plexiglas capsules with a 15-mm-diam disk and a 5-mm-ID cylinder were affixed to the visceral pleura with cyanoacrylate glue, and three or four holes, ~1–2 mm deep, were made in each capsule by gently twirling a conical pin of 0.8 mm maximum diameter. Capsule pressures were measured with catheter-tip transducers (Mikro-Tip, Millar Instruments, Houston, TX). The catheters were coiled and suspended so that they exerted minimal load on the lung surface. In *dogs 1* and *2* one capsule was placed on each middle lobe, whereas in *dogs 3–6* two capsules were affixed to one of the middle lobes, as close as possible but without touching each other at end expiration, and a third capsule was placed on the opposite lobe.

Tracheal flow ($\dot{V}$) was measured with a heated screen pneumotachograph and a Validyne MP-45 (±5 cmH_2O)

transducer. Airway opening pressure (Pao) was sensed with another MP-45 (±30 cmH_2O) transducer through a side tap of the tracheostomy tube. The frequency responses of the flow- and pressure-measuring channels, including the sensors, the amplifiers, and the 0.1- to 25-Hz band-pass filters, were recorded while the transducers were exposed to the same dynamic pressure field; then, with reference to the flat-response (0- to 20-kHz) Mikro-Tip sensors, the Pao and $\dot{V}$ signals were corrected in the preprocessing phase for amplitude and phase deviations.

Forced oscillations. The volume oscillations were produced with a closed-box loudspeaker system, described in detail previously (9). The loudspeaker was driven via an analog-digital board and a power amplifier by a VT-110 (Videoton, Hungary) IBM XT-compatible computer, which was also used for the processing of the measured signals. The pseudorandom driving signal (U) was specified as follows: it had a repetition time of 20 s, but the fundamental component (0.05 Hz) was missing. The first nonzero component was 0.1 Hz, and the other components (0.15, 0.25, 0.35, 0.55, . . . 20.45 Hz) were prime number multiples of the fundamental and were selected so that they were spaced as evenly as possible on the log frequency scale. The fact that any component was a noninteger multiple of the lower-frequency ones ensured that the harmonics produced by possible nonlinearity could not interfere with the components of U, and, consequently, neither the impedance nor the coherence estimates were biased through the production of harmonics (4). The component amplitudes were specified so that the power spectrum of U decreased hyperbolically with frequency, and the component phase angles were then optimized to attain the minimum amplitude of the composite signal at the prescribed total power (5). This optimization, together with the attenuation of the higher-frequency components, was aimed at minimizing the involvement of nonlinear phenomena in the airways. The loudspeaker acted as a volume generator: the volume delivered was proportional to U, almost independently of the measured Z_L, and amounted to 43 ± 3 ml peak to peak; this corresponded to $\dot{V}$ values < ±220 ml/s.

Protocol. Each oscillatory measurement started 4–5 s after the animal had been disconnected from the respirator at end expiration and lasted for 30 s. Between measurements, the lung was slightly hyperinflated by occluding the expiratory outlet of the respirator for one breathing cycle to avoid atelectasis and also to increase the animal's ability to tolerate the suspension of ventilation. Immediately before the tracheal tube was connected to the loudspeaker through the pneumotachograph, the loudspeaker chamber was pressurized to 5 cmH_2O, i.e., the transpulmonary pressure at which the measurement was made. After the oscillation recordings had been made in the control state, the measurements were repeated during intravenous infusion of histamine (8 $\mu g \cdot kg^{-1} \cdot min^{-1}$) in an interval when the blood pressure had reached a steady state again. Eight measurements were recorded in each condition.

Computations. The signals of $\dot{V}$, Pao, and P_{A_i} were sampled at 102.4 Hz, and the input impedance (Z_L = Pao/$\dot{V}$), tissue (transfer) impedances ($Ztr_i = P_{A_i}/\dot{V}$), and airway (transfer) impedances ($Zaw_i = Z_L - Ztr_i$) were computed from the cross-power spectra (G_{xU}) of every measured signal x with U (10). (It should be stressed that neither Ztr_i nor Zaw_i corresponds to local tissue or airway impedances because of the lack of concurrently measured local flows: they should therefore be interpreted rigorously as transfer quantities measured in a one-input multiple-output system.) The estimates of G_{xU} were obtained with fast Fourier transformation with time blocks of 20 s, according to the periodicity of U. Because the recordings were only 1.5 periods long, the number of time blocks necessary for the reliable estimation of G_{xU} spectra was increased to nine by using 93.75% overlapping. As indexes of reliability, the coherence functions γ^2_{xU} were computed; recordings in which any γ^2_{xU} had values <0.98 (except at the heart frequency and its harmonics) were rejected. This coherence criterion was fulfilled in at least six of the eight recordings in each series, the corresponding impedances and transfer functions of which were ensemble averaged. All impedances (Z) are expressed in terms of real (R) and imaginary parts (X), and indexed according to Z.

Models. The Z_L data between 0.1 and 4.15 Hz were evaluated on the basis of the following models in which invariably $Z_L = Zaw + Zti$ and $Zaw = Raw + j\omega Iaw$ were assumed (Raw and Iaw denote airway resistance and inertance, respectively; j is the imaginary unit, and ω is angular frequency). In accordance with Hildebrandt's model (13), which described the impedance on the basis of the logarithmic stress relaxation process observed in excised cat lungs, in *model 1* Zti was expressed as

$$Zti = D\pi/4.6\omega - j(C + 0.25D + D \log \omega)/\omega$$

where D is the coefficient of the tissue real part (damping), also determining the frequency dependence of the elastance, the value of which is given by $C + 0.25D$ at $\omega = 1$. In *model 2* Zti is assumed to be a constant-phase impedance, wherein the real and imaginary parts decrease with the same power (α) of ω (12)

$$Zti = (G - jH)/\omega^{\alpha}$$

where G and H are again coefficients for damping (viscance) and elastance, respectively. In the time domain, the above expression describes the decay of pressure $p(t)$ after the volume increment V_T as $p(t)/V_T = At^{-k}$, where A and k are constants. With the assumption of an asymptotic value B, the stress relaxation process is described as $p(t)/V_T = At^{-k} + B$; this latter formula was used by Hildebrandt to fit the pressure decays observed in a rubber balloon (13).[1]

[1] According to Hildebrandt (13), Laplace transformation of this process results in the expression of the elastic modulus: $T(s) = sP(s)/V_T = As^k\Gamma(1 - k) + B$, where $s = j\omega$ and $\Gamma(1 - k)$ is the gamma function of $(1 - k)$. Dividing T(s) by s, we obtain the expression of impedance Zti(s). Let $\alpha = 1 - k$. We then obtain the following form: $Zti(j\omega) = A\Gamma(\alpha)[(\cos(\alpha\pi/2) - j \sin(\alpha\pi/2)/\omega^{\alpha}] - jB/\omega$, which includes three parameters (A, α, and B). Instead of A and α, we can introduce the parameters G and H as coefficients for the real and imaginary parts, respectively, as follows: $G = A\Gamma(\alpha) \cos(\alpha\pi/2)$ and $H = A\Gamma(\alpha) \sin(\alpha\pi/2)$. Note that the exponent α can be expressed as $\alpha = (2/\pi) \arctan(H/G)$ and is, therefore, not an independent parameter. Neglect of the asymptotic value B leads to the formula of the constant-phase impedance.

The parameters of the above models were obtained by minimizing the objective function

$$F = \{(1/m) \sum_{j=1}^{m} [|Z_L(\omega_j) - Z_L'(\omega_j)|^2/|Z_L(\omega_j)|^2]\}^{1/2}$$

where $Z_L(\omega_j)$ and $Z_L'(\omega_j)$ denote the measured and modeled impedance values, respectively, at frequencies ω_j ($1 \leq j \leq m$). Data corresponding to the heart frequency and its harmonics were often scattered; when they yielded deviating mean values in the repetitive measurements, these points were discarded in the fitting procedure. To make the tissue parameters of the two models comparable, we calculated damping and elastance at $\omega = 1$ for *model 1* as $G = D\pi/4.6$ and $H = C + 0.25D$, respectively. Tissue hysteresivity (η) was calculated as $\eta = G/H$ (8).

Simulations. We considered a simplified lung structure proposed by Fredberg et al. (7); a central airway impedance (Zcaw) with resistive (Rcaw) and inertive (Icaw) parameters was connected to n parallel peripheral branches (Fig. 1). As a first step, the parallel resultant of the branch impedances, i.e., the equivalent one-compartment peripheral impedance (Zp), was specified by establishing the peripheral airway parameters Rpaw, Ipaw, and the tissue parameters G and H of *model 2*. Then, Zp was split into parallel branches (for computational reasons the actual value of n was 900), and random values, approaching uniform distributions in terms of admittance, were given independently to the parameters of the peripheral airway branch impedances $Zpaw_i$ ($Rpaw_i$ and $Ipaw_i$) and the tissue impedances Zti_i (G_i and H_i).[2] For simplicity, the ratios $Ipaw_i/Rpaw_i$ and G_i/H_i were kept constant in all branches. The airway wall distensibility was represented by a shunt compliance (Cb) connected in parallel with the peripheral units.

RESULTS

Measured data. The values of pulmonary resistance (R_L) and tissue (transfer) resistances (Rtr_i) estimated in *dogs 3–6*, in which three local P_{A_i} signals were measured, are shown in Fig. 2 (in the first 2 experiments, where only 2 capsules were used, the results were qualitatively similar to the others). In the control state, most Rtr_i curves run parallel with that of the corresponding R_L, which suggests that the estimates of Raw are roughly frequency independent. During histamine infusion (HI), the low-frequency R_L values increased to 140–280% of the control; in several Rtr_i curves, the frequency dependence was changed profoundly (*dogs 3* and *6*), which implies marked decreases in the local estimates of Raw ($Raw_i = R_L - Rtr_i$) with frequency. In these cases, Rtr_i crossed zero and remained negative for shorter or longer intervals of frequency, which corresponds to "paradoxical looping" in the P_{A_i} vs. Pao relationship (6). The effective pulmonary elastance, calculated from the reactance (X_L) as $E_L eff = |\omega X_L|$, followed a fairly linear increase on the log frequency scale up to 0.5–1 Hz and then declined as a result of the dominating effect of inertive forces (Fig. 3). HI increased $E_L eff$; the elevations at low frequencies amounted to 17–57% of the control. The elastances calculated from Ztr_i (Etr_i) increased linearly and uniformly up to 5 Hz in most of the control cases and also in a few cases during HI (*dogs 4* and *5*). At higher frequencies there were fluctuations, probably due to local pathway resonances, and departures of the Etr_i curves within each dog. The heterogeneity of P_{A_i} is nevertheless indicated by the differences in Rtr_i, even at low frequencies in the control state, and is shown to be increased by histamine in both Rtr_i and Etr_i (Figs. 2 and 3). The largest intraindividual differences in Rtr_i and Etr_i do not relate exclusively to data obtained from opposite lobes, because in *dog 3* (control) and in *dogs 3* and *4* (HI) the differences between adjacent capsules were the largest.

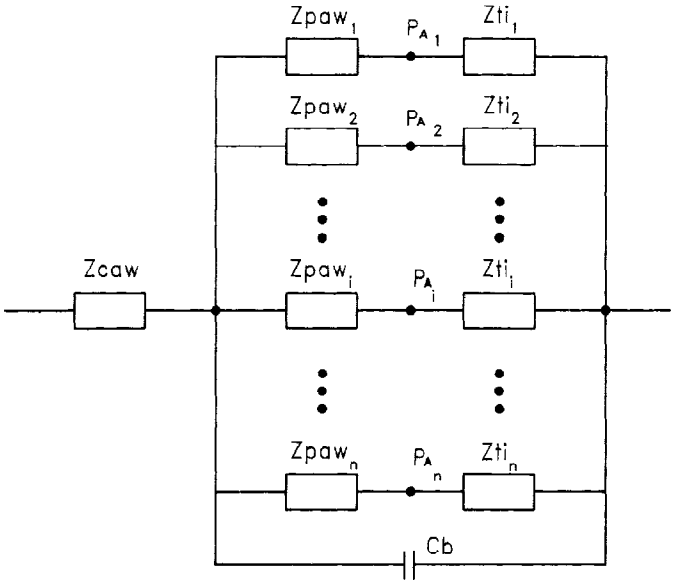

FIG. 1. Distributed-periphery model for simulation of pulmonary impedance consisting of lumped elements for central airway impedance (Zcaw) and bronchial compliance (Cb) and impedances of peripheral airways ($Zpaw_i$) and tissue units (Zti_i) with values of independent distributions. P_{A_i}, local alveolar pressures.

The residual errors of fitting, i.e., the normalized differences $(R_L - R_L')/|Z_L|$ and $(X_L - X_L')/|Z_L|$, are averaged for all Z_L data and plotted against frequency in Fig. 4. *Model 2* provided smaller and less systematic deviations from the measured data than did *model 1*: the average residuals were within the ranges of ±1 and ±0.6% for the real and imaginary parts, respectively. The results of parameter estimation from the Z_L data are summarized in Table 1. When *model 1* was used instead of *model 2*, the fitting errors increased by 35 and 66% in the control and during HI, respectively, and systematically higher Raw and lower Iaw values were found. Slight differences in G, H, and η were also observed. Marked histamine-induced elevations in Raw, G, H, and η were revealed by both models, although the highly variable individual responses of Raw did not result in a statistically significant average increase. The change in Iaw was opposite and less significant (<10%) in the case of *model 2*.

Figures 5 and 6 show typical measured R_L and E_L data, respectively, together with the fitting curves of the mod-

[2] Subscript i refers to values assigned to (or computed for) the ith peripheral branch in the simulation model ($1 \leq i \leq n$), and it is also used to index the measured local alveolar pressures and the quantities computed therefrom ($i = 1, 2, 3$).

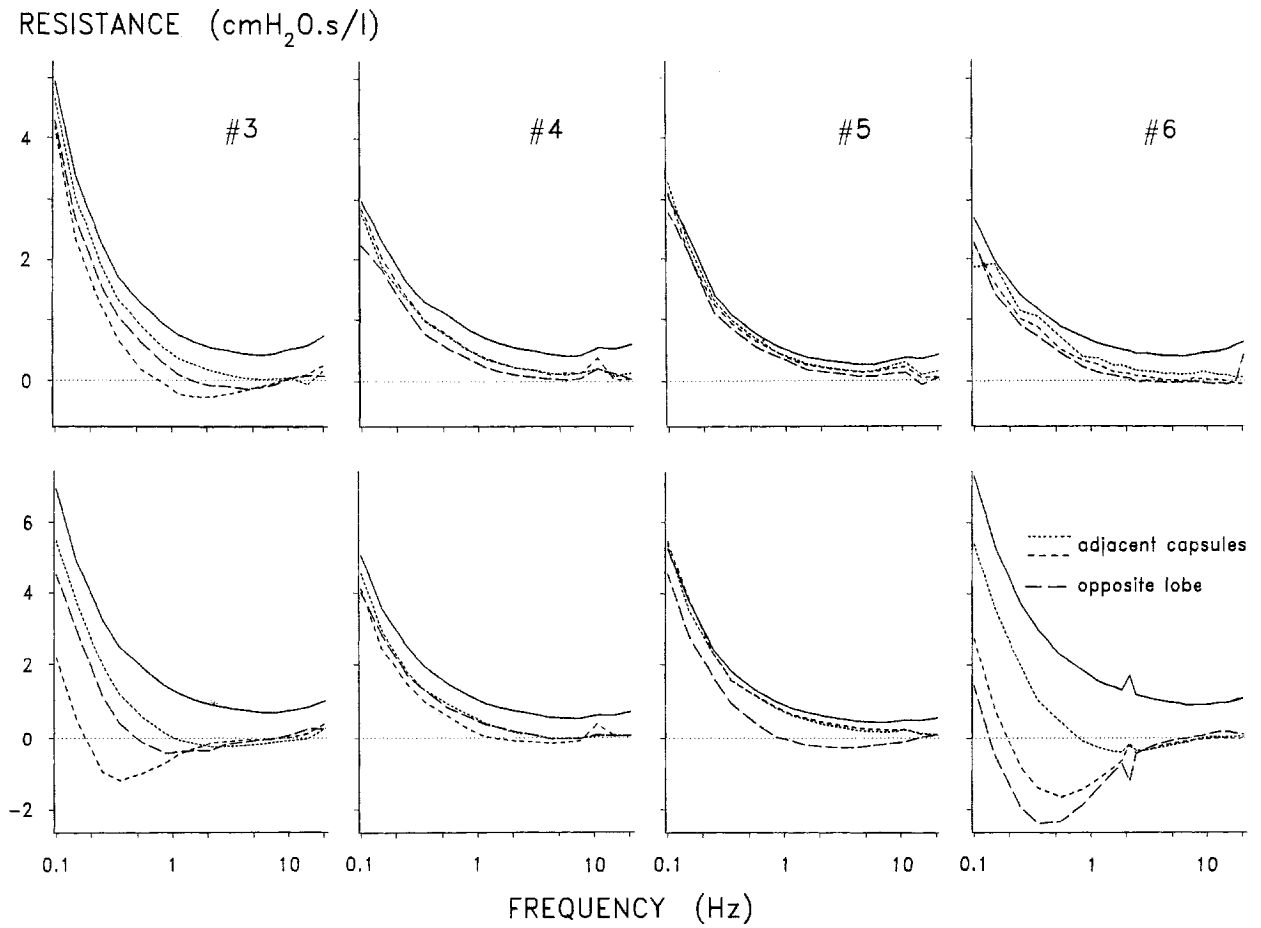

FIG. 2. Real parts of pulmonary input impedance (solid line) and tissue (transfer) impedances (dashed lines) vs. frequency in 4 dogs in control (*top*) and during histamine infusion (*bottom*). Note different scale in *bottom panels*. Values are means of 6–8 measurements in each condition.

els. To enhance the deviations from the strictly hyperbolic decrease in RL with frequency, which is inherent in the *model 1* formulation, the RL data were plotted against the reciprocal of frequency (Fig. 5). The fact that the RL data appear in a slightly curved fashion accounts for most of the improvement in fitting provided by *model 2*. This is particularly true for the HI data, where the higher η values obtained (Table 1) reflect a lower value of the exponent α, which decreased from the control value of 0.911 ± 0.013 to 0.878 ± 0.009. The EL values (Fig. 6) were calculated from XL by subtracting the inertial reactance first, i.e., $EL = \omega|(XL - \omega Iaw)|$. Hence, the sets of inertance-corrected EL data are slightly different, depending on the model type used; those estimated by *model 2* fittings exhibit a slight upward deflection with log frequency, whereas the higher Iaw values given by *model 1* lead to a more linear arrangement of the EL data. In accordance with the data presented in Table 1, the histamine-induced elevations of RL and EL were associated with invariably good fittings by *model 2*.

The Zaw_i data displayed a great variability within each dog and also in their interindividual changes due to HI. As exemplified in Fig. 7, Raw_i was largely frequency independent up to 5–10 Hz, and Xaw_i increased with frequency in a fairly linear manner in the majority of the control measurements (in 10 of the 16 cases). In the remaining control Zaw_i data and in 14 cases of the HI measurements, Raw_i exhibited a marked negative frequency dependence at low frequencies, which was associated with a downward bend of Xaw_i before its return to the linear increase. The Raw_i data pooled at 0.25, 4.15, and 10.55 Hz, respectively, amounted to 184 ± 99, 133 ± 46, and 134 ± 39% (SD) (control) and to 351 ± 202, 148 ± 43, and 126 ± 32% (HI) of the corresponding Raw values from the *model 2* fitting in the 0.1- to 4.15-Hz interval. In all data groups, the differences between Raw_i and Raw were significant ($P < 0.01$) by the paired t test.

Simulated data. The one-compartment parameters of the simulation model (Fig. 1) were initially set to correspond to typical estimated values from the control measurements of ZL. After splitting Zp into parallel branches, the $1/Zpaw_i$ values (i.e., peripheral airway admittances) were given an even distribution between 5 and 100% of the maximum $1/Zpaw_i$. The range of distribution of tissue admittances ($1/Zti_i$) was ±25% around their average value. Peripheral bronchoconstriction was simulated by increasing Rpaw from 0.1 to 0.4 and 0.8 $cmH_2O \cdot s \cdot l^{-1}$ while preserving the initial distributions, i.e., elevating the $Rpaw_i$ values proportionally in all branches. For the sake of clarity, all other parameters were fixed, at Rcaw = 0.2 $cmH_2O \cdot s \cdot l^{-1}$, Icaw = 0.02 $cmH_2O \cdot s^2 \cdot l^{-1}$, Ipaw = 0.002 $cmH_2O \cdot s^2 \cdot l^{-1}$, G = 2.4 cmH_2O/l, and H = 16 cmH_2O/l. As shown in Table 2, the fitting of the one-compartment model to the simulated

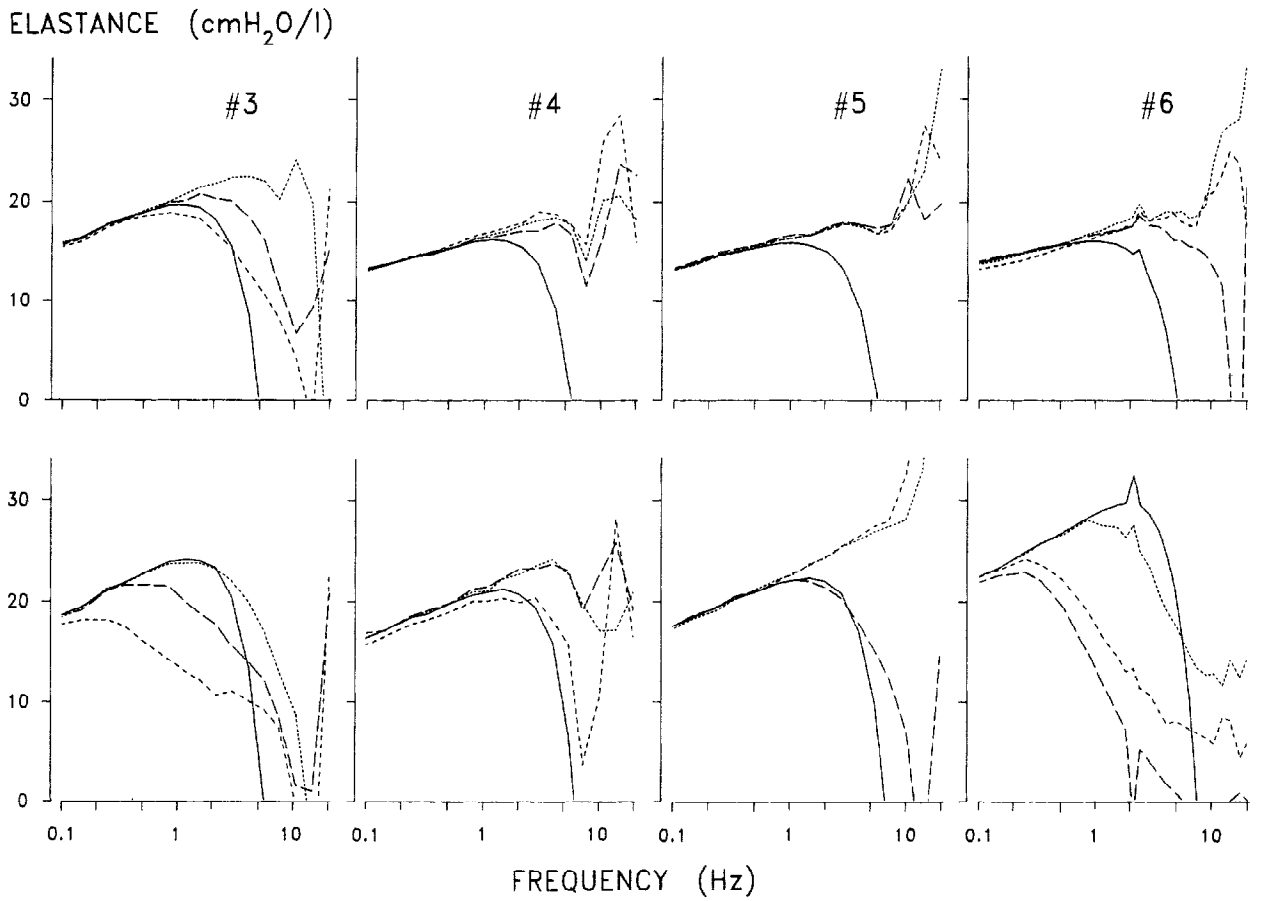

FIG. 3. Effective elastances calculated from pulmonary input impedance (solid line) and tissue (transfer) impedances (dashed lines) vs. frequency in 4 dogs in control (*top*) and during histamine infusion (*bottom*). Values are means of 6–8 measurements in each condition.

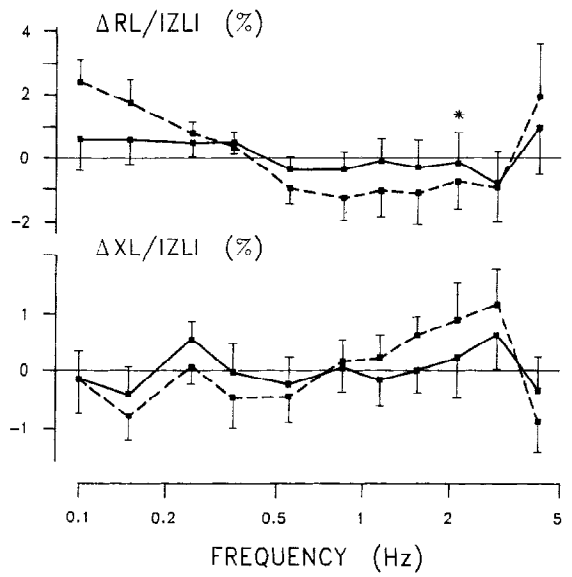

FIG. 4. Fitting errors of *models 1* (dashed line) and 2 (solid line), expressed as differences between modeled and measured values of pulmonary resistance (RL) and reactance (XL), normalized by impedance magnitude (|ZL|). Values (means ± SD) are from pooled data obtained in control and during histamine infusion (n = 12). *Two data points were discarded in fitting.

ZL data in the range of 0.1–4.15 Hz resulted in gradually increasing fitting errors with the elevation of Rpaw, although at Rpaw = 0.8 $cmH_2O \cdot s \cdot l^{-1}$ they were still comparable with the F values obtained in the actual measurements. The one-compartment parameters Raw = Rcaw + Rpaw, Iaw = Icaw + Ipaw, and G were progressively underestimated with increasing Rpaw, whereas H remained constant; consequently the 18% change in the apparent η was due to the elevation of G alone.

Putting the lumped bronchial compliance (Cb) with a value of 0.002 l/cmH_2O [which is 2.5 times lower than that assumed for the human bronchial system by Mead (19)] in parallel with the peripheral branches did not cause qualitative changes in the simulated ZL, Ztr_i, and Zaw_i data. As indicated by the F values, *model 2* fitted ZL invariably well, and there were only slight decreases in the parameter estimates.

The effect of increasing Rpaw on Ztr_i is illustrated in the case of three groups of peripheral branches, with $Rpaw_i$ close to the minimum, average, and maximum values of the distribution. Each group consisted of three branches that ended in a Zti_i of low, medium, or high value. Elevation of Rpaw augmented the differences between the Rtr_i curves (Fig. 8) and shifted the separation of the Etr_i graphs toward lower frequencies (Fig. 9). These patterns resemble the changes seen in the measured Rtr_i values (cf. Figs. 2 and 3). It is remarkable that the influence of the changes in Zti on both Rtr_i and Etr_i were small and discernible only for the highest-resistance pathways.

In Fig. 10, two families of simulated Zaw_i curves are

TABLE 1. *Values of model parameters and fitting errors*

Model	F, %	Raw, $cmH_2O \cdot s \cdot l^{-1}$	Iaw, $cmH_2O \cdot s^2 \cdot l^{-1}$	*G*, cmH_2O/l	*H*, cmH_2O/l	η
			Control			
1	1.46±0.59	0.347±0.123	0.0161±0.0041	2.28±0.551	15.23±2.05	0.149±0.024
2	1.08±0.37	0.317±0.120	0.0169±0.0043	2.19±0.501	15.46±2.09	0.141±0.021
P	<0.02	<0.01	<0.01	<0.01	<0.001	<0.01
			Histamine			
1	1.90±0.78	0.839±0.500	0.0130±0.0063	4.31±0.80	20.59±2.78	0.208±0.016
2	1.14±0.52	0.749±0.475	0.0153±0.0061	4.14±0.81	20.99±2.85	0.196±0.016
P	<0.01	<0.001	<0.001	<0.001	<0.001	<0.001
*P**	NS	NS	<0.05	<0.01	<0.01	<0.01
P†	NS	NS	NS	<0.01	<0.01	<0.01

F, fitting error; Raw, airway resistance; Iaw, airway inertance; *G* and *H*, coefficients of the real and imaginary parts of tissue impedance, respectively; η, hysteresivity index. * Differences in *model 1* values between control and histamine. † Differences in *model 2* values between control and histamine.

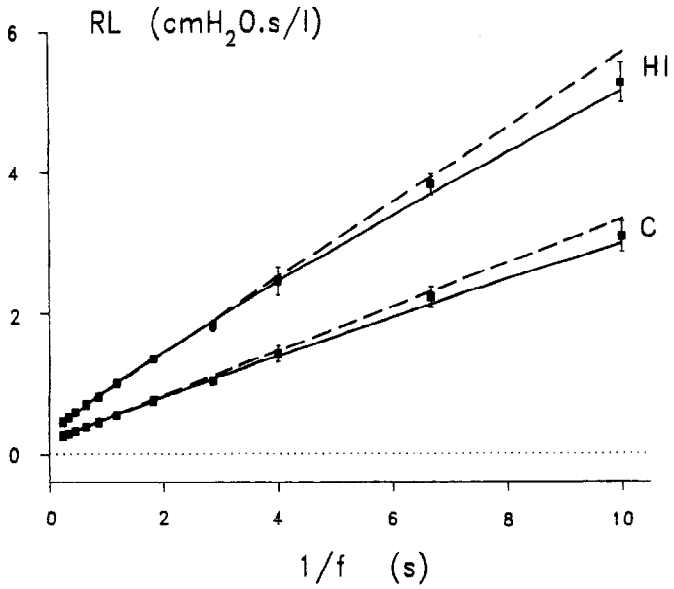

FIG. 5. Real part (RL) of pulmonary input impedance vs. reciprocal of frequency ($1/f$) in control (C) and during histamine infusion (HI) in 1 dog. Values (means ± SD) are from 6 measurements in each condition. Fittings of *models 1* and *2* are illustrated with dashed and solid lines, respectively.

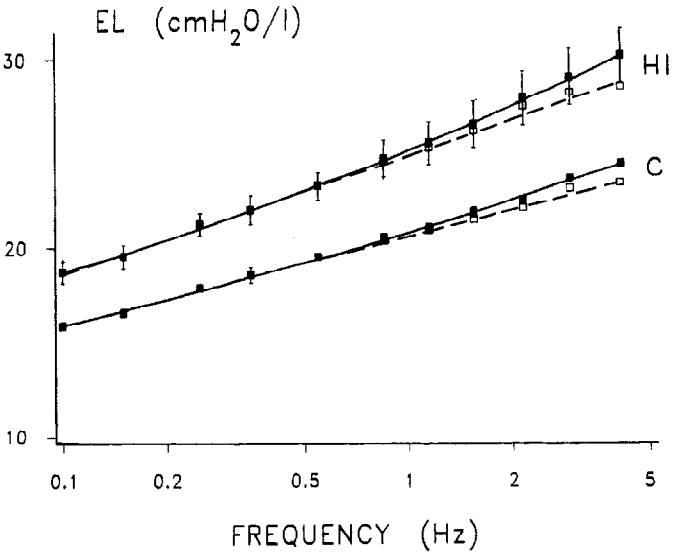

FIG. 6. Pulmonary elastance (EL) calculated from imaginary part of input impedance, with removal of inertial reactance obtained from fitting of *models 1* (open symbols) and *2* (closed symbols) in frequency range 0.1–4.15 Hz. Values (means ± SD) are from 6 measurements in control (C) and during histamine infusion (HI) in one dog. Dashed and solid lines, tissue elastance from fitting of *models 1* and *2*, respectively.

shown from the population generated with the same one-compartment initial parameters and distributions as in the preceding study. The Raw_i curves start from different values, depending on $Rpaw_i$, and run fairly parallel up to 5 Hz in the case of low resultant Rpaw, whereas those relating to high Rpaw (with the exception of the minimum-resistance pathway) join rapidly with increasing frequency. Xaw_i departs more from the linear increase of the one-compartment airway reactance, the higher $Rpaw_i$ pathway considered. The drastic fall in Xaw_i calculated from the high-resistance branches for an elevated overall Rpaw is similar to those frequently found during HI (see Fig. 7).

DISCUSSION

Regional inhomogeneity. The alveolar capsule technique has been shown to give reliable estimates of the local alveolar pressures under strict methodological conditions (1–3, 6, 7, 15–18, 20–24) and has been used to assess the inhomogeneity of alveolar pressure during oscillations at different frequencies (1, 3, 6, 7, 15, 22, 24), deflations at maximal (16, 18, 21) and submaximal flows (24), and rapid flow interruptions (2, 20). It should be emphasized, however, that the limited availability of measurement sites precludes systematic studies on regional inhomogeneity, even if the latter is understood specifically in terms of interlobar (e.g., apex-to-base) differences (1). From this, it follows that the documented differences in P_{A_i} are indicative only of an appreciable inhomogeneity, and neither the mean PA nor a statistically reliable indicator of the overall pressure variability can be estimated from a few measurement sites.

At low frequencies, where Zaw is a small fraction of ZL, the magnitude of P_{A_i} ($|P_{A_i}|$) is expected to exhibit minor spatial variations and approach the value of |Pao| (1, 6, 7), and this should be almost independent of whether Zti

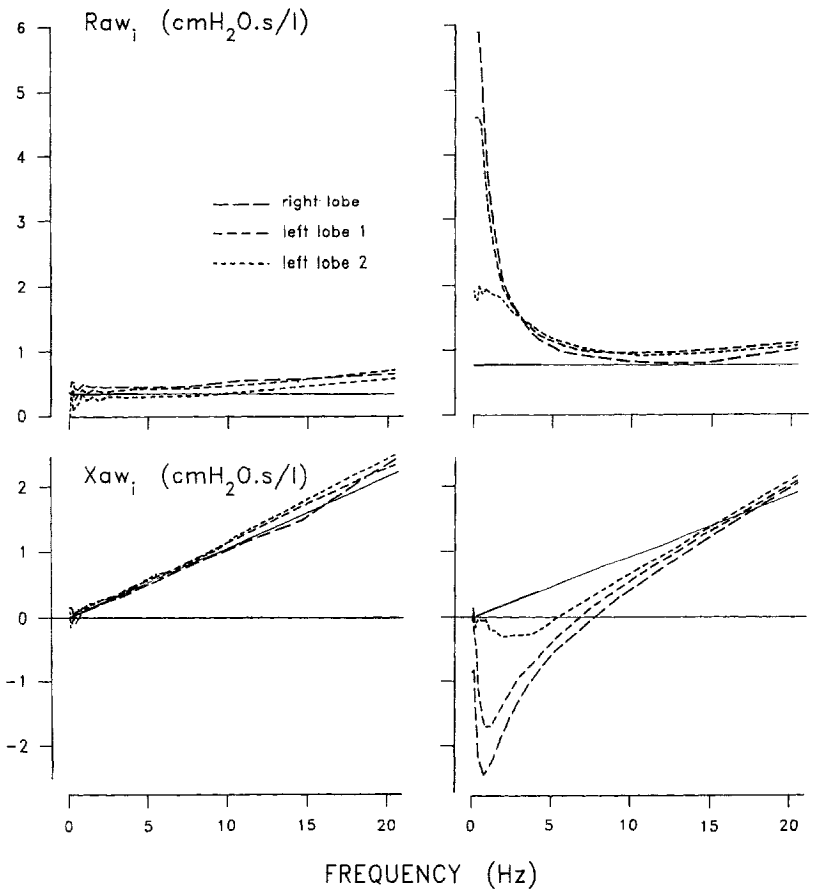

FIG. 7. Typical patterns of "airway" impedances estimated from measurements of local alveolar pressures, in terms of real (Raw_i) and imaginary parts (Xaw_i), in the control (*left*) and during histamine infusion (*right*). Solid lines, Raw and Xaw obtained from input impedance fittings by *model 2* in range 0.1–4.15 Hz.

is uniform throughout the lung. Accordingly, in the present study the variability of $|Ztr_i|$ (which is equal to that of $|P_{A_i}|$, because the same central flow $\dot{V}$ is used in the calculation of Ztr_i) was extremely small at 0.1 Hz; the coefficient of variation (CV) was 1.1% in the control and 3.5% during HI, with negligible differences between |Pao| and $|P_{A_i}|$. At the same time, however, the corresponding CV values of Rtr_i amounted to 8.7 and 82.6%, respectively. This fact is in accordance with previous findings (3, 23) and implies that considerable phase differences exist between regional lung units, which may give rise to intense interregional flows even in the case of the fairly uniform $|P_{A_i}|$ values prevailing at 0.1 Hz. On inspection of our Rtr_i and Etr_i data shown in Figs. 2 and 3, it is apparent that with increasing frequency the enhancement of phase differences is associated with progressive heterogeneity in $|P_{A_i}|$. Indeed, at 4.15 Hz the CV of $|Ztr_i|$ increased to 13 (control) and 32% (HI) and $|Ztr_i|$ amounted on average to 116 and 57% of $|Z_L|$, in the control and during HI, respectively. The latter values indicate that at 4.15 Hz (i.e., somewhat below the resonant frequency of 5–6 Hz in the control) $|P_{A_i}|$ exceeded |Pao|, a phenomenon described as the resonant amplification of P_A (7), whereas during HI the increase of Raw led to the overall damping of P_A. These findings are in accordance with both the diversification of the magnitude and phase of the individual P_{A_i}/Pao ratios with increasing frequency and their histamine-induced alterations, described in a higher-frequency range (1, 6, 7).

Input impedance. The marked fall in R_L and the slight increase in E_L as frequency increases are in agreement with earlier observations at low frequencies (3, 9, 11–15,

TABLE 2. *Results of one-compartment model fitting to simulated distributed-periphery data*

Rpaw, $cmH_2O \cdot s \cdot l^{-1}$	F, %	Raw, $cmH_2O \cdot s \cdot l^{-1}$	Iaw, $cmH_2O \cdot s^2 \cdot l^{-1}$	G, cmH_2O/l	H, cmH_2O/l	η
			Cb = 0			
0.1	0.09	0.308	0.0215	2.39	16.00	0.150
0.4	0.57	0.542	0.0196	2.56	15.98	0.160
0.8	1.13	0.801	0.0184	2.84	16.00	0.177
			Cb = 0.002 l/cmH$_2$O			
0.1	0.10	0.294	0.0213	2.25	15.52	0.145
0.4	0.53	0.503	0.0194	2.40	15.50	0.155
0.8	1.06	0.729	0.0180	2.64	15.53	0.170

Cb, bronchial compliance; Rpaw, specified resultant peripheral airway resistance; F, fitting error; Raw, airway resistance; Iaw, airway inertance; G and H, coefficients of the real and imaginary parts of tissue impedance, respectively; η, hysteresivity index. See text for other specified values and further explanation.

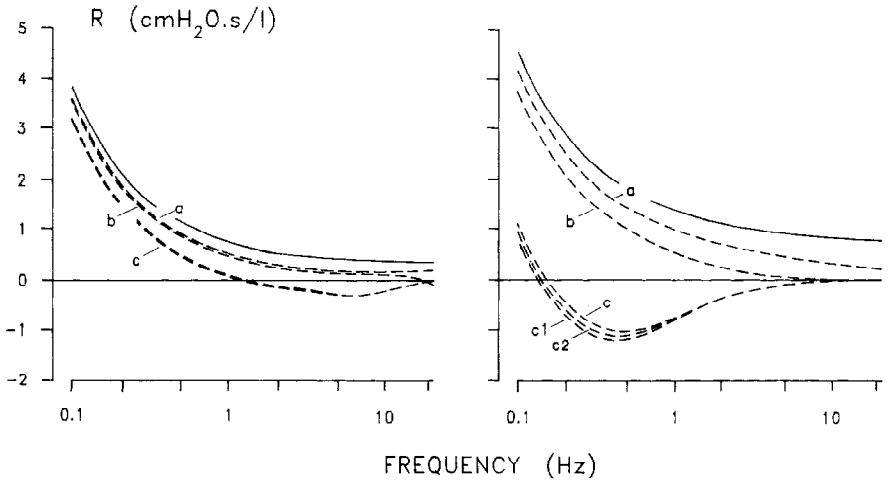

FIG. 8. Real parts (R) of simulated pulmonary input impedance (solid line) and tissue (transfer) impedances (dashed lines) vs. frequency with result of peripheral airway resistances ($Rpaw_i$) set at 0.1 (*left*) and 0.8 $cmH_2O \cdot s \cdot l^{-1}$ (*right*). *Curves a, b,* and *c* relate to peripheral branches with minimum, average, and maximum $Rpaw_i$, respectively. Data corresponding to minimum (*c1*), average (*c*), and maximum (*c2*) tissue impedances depart from each other only in the case of maximum $Rpaw_i$.

22). The changes in ZL due to the infusion of histamine, assessed either from those in RL and EL in a model-independent manner (Figs. 5 and 6) or on the basis of model parameters (Table 1), showed that at frequencies around the spontaneous breathing rate the elevation in ZL is overwhelmingly due to that in Zti, and the contribution of the increased Raw to the dissipative losses becomes significant only in the upper half of the frequency region investigated. These findings are partly in agreement with the responses to aerosolized histamine in previous studies (6, 14, 15, 20), where the elevation in Rti was a significant or even predominant component of the rise in RL, depending on the histamine dose and the frequency of deformation. Recently, it has also been shown that the histamine responsiveness of the peripheral airways and lung tissues may be markedly different between dogs and within lung regions (17).

Both models provided good fits to the measured ZL data, in the control and during HI. Although analysis of the fitting quality in terms of residuals disclosed a slight overestimation of RL at low frequencies in the case of *model 1,* the values of F are about half of those found previously under similar experimental conditions (9), where in turn significant systematic differences between measured and modeled ZL data, if any, were not detectable within the wider scatter of residuals. Because the present study differs from the previous one (9) only in the spectral content of the applied driving signal (quasi-equidistant spacing of components on the log frequency scale between 0.1 and 20.45 Hz, instead of the inclusion of every multiple of 0.125 Hz up to 5 Hz), the reason for the changed fitting behavior of *model 1* is really not clear. Reevaluation of ZL data from our previous work (9) nevertheless indicated that among the densely spaced higher-frequency data points many more ZL data were affected by the cardiac noise than those omitted from model fitting, and this may offer an explanation for the higher F values found previously. Another factor leading to smoother data is the exclusion of multiple-frequency components of the driving signal, which has been shown to reduce the effect of nonlinear harmonic production (4). At any event, in the current study, the fits given by *model 2* are convincingly better than those given by *model 1* and are equally good in both measuring conditions, and therefore in the simulation model the Zti described by *model 2* was favored. Because of the similar descriptions of the tissue mechanics, however, the conclusions drawn from the simulation study would be practically the same with either model.

The constant-phase model is rigorously compatible with the structural damping hypothesis (8), whereby the dissipative and elastic processes are coupled at the elementary level of the lung tissue. The specific mechanisms that may underlie phase constancy remain speculative (8), but at the phenomenological level it is important to note that *model 2* arises from a rate-dependent relax-

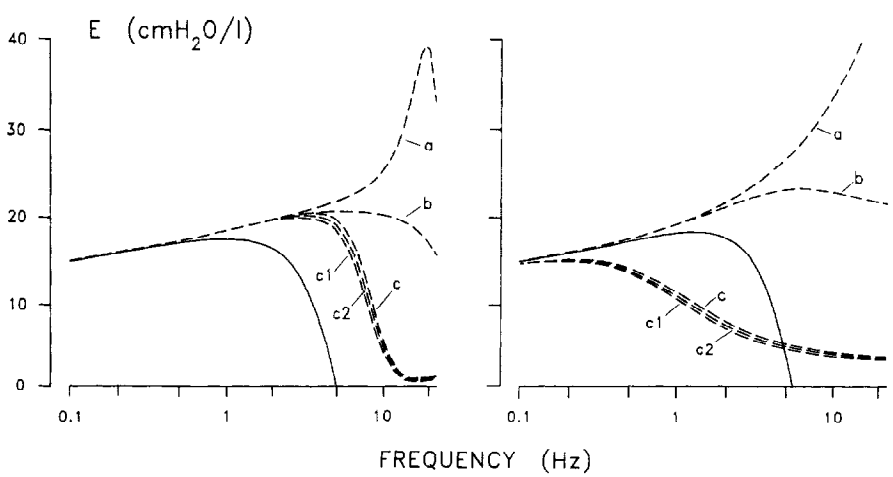

FIG. 9. Elastances (E), i.e., imaginary parts times angular frequency, from the same simulation study as in Fig. 8. See text and legend to Fig. 8 for further explanation.

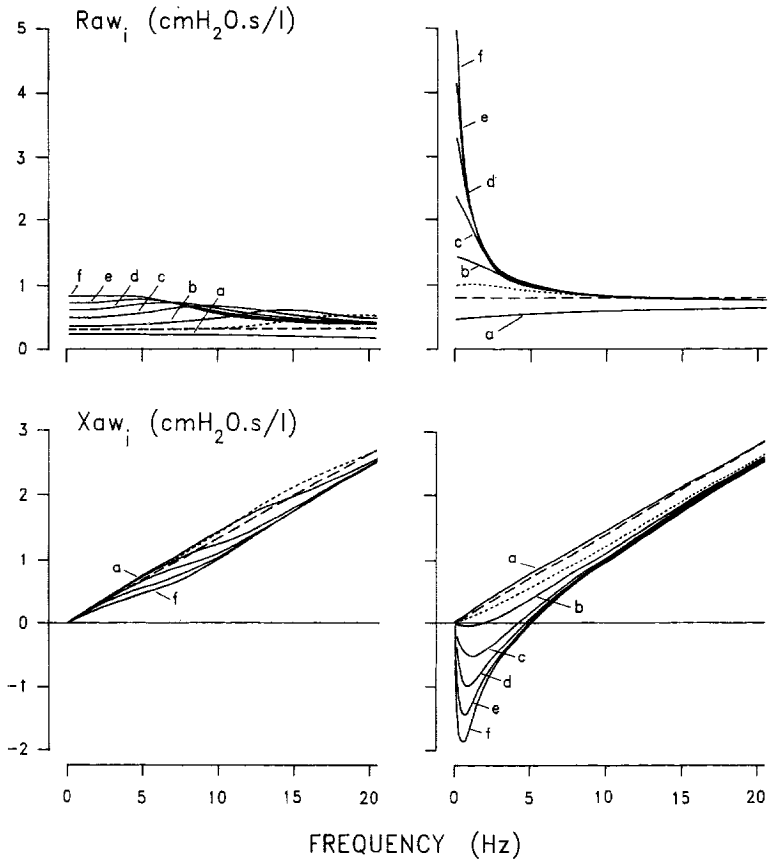

FIG. 10. Real (Raw) and imaginary (Xaw) parts of simulated "airway" impedances vs. frequency with nearly equal increments from minimum (*a*) to maximum (*f*) value of peripheral airway resistance, all ending at medium values of local tissue impedance. Dashed lines, Raw and Xaw estimated from simulated pulmonary impedance by *model 2* fitting. Simulation parameters are the same as in Fig. 8. *Left* and *right*: resultant peripheral airway resistance of 0.1 and 0.8 $cmH_2O \cdot s \cdot l^{-1}$, respectively.

ation equation. Accordingly, *model 2* provides a clear counterexample that the structural damping phenomenon is not restricted to plastic or rate-independent mechanisms of energy dissipation. Although structural damping may describe certain plastic or viscoelastic processes, it implies neither.

The frequency-domain formulations of both models are derived from empirical fitting formulas describing stress relaxation processes after a sudden change in volume (13), and hence their validity is expected only within the time interval (or the corresponding frequency range) of the measurement. Nevertheless it may be informative as to how the tissue parts of these models behave at extreme values of time or frequency. *Model 1* assumes a pressure decay of the form $p(t)/V_T = C - D \log t$ (13) and, therefore, becomes physically uninterpretable not only at $t = 0$ (infinitely high frequency) but also when the observation time reaches $\log t = C/D$, although the latter discrepancy appears only above 10^3–10^4 s (i.e., below 10^{-3}–10^{-4} Hz), according to the highest h values (0.25 – 0.3) reported so far (8). By contrast, *model 2* predicts that with decreasing frequency Rti and Xti tend monotonously to plus and minus infinity, respectively, whereas the time-domain formula shows that $p(t)$ approaches zero with increasing t. The disappearance of pressure (i.e., the lack of a loss-free elastic element) can be remedied formally by putting the asymptotic value B of $p(t)/V_T$ back into *model 2*, thereby returning to the rubber balloon model of Hildebrandt (13). In the frequency-domain formula of the latter, B corresponds to an ideal (hyperbolic) elastic reactance ($B/j\omega$) added to the constant-phase component $H/j\omega^{\alpha}$. With this additional parameter included, our ZL data could be fitted at decreased F values: 0.74 vs. 1.08% ($P < 0.05$) and 0.92 vs. 1.14% ($P < 0.01$) in the control and during HI, respectively. However, although the sums $H + B$ were almost identical with the H values from *model 2*, the estimates of B were enormously variable: they ranged from −17.22 to 10.36 cmH_2O/l in the control and from −10.77 to 11.42 cmH_2O/l during HI. This indicates that the frequency range of our ZL data was not wide enough to obtain stable and physically meaningful values for this additional parameter.

On the other hand, the restriction of the model fitting to the frequency interval from 0.1 to 4.15 Hz enabled us to neglect the effects of other parameters, such as those describing the frequency dependence of Raw and Iaw, and to avoid the involvement of tissue inertance. As a consequence of the latter, the impedance of the alveolar gas compressibility (Zg) cannot exert an appreciable shunt effect on Zti, because Zg is much greater than, and similarly frequency-dependent as, Zti. The negligible influence of Cb on the recovered values of the tissue parameters (Table 2) can be explained analogously; as long as the impedance distal to the shunt point is characterized by an approximate inverse proportionality to frequency, the frequency dependence of RL and EL will not be qualitatively different from that of Rti and Eti. Consequently, at low frequencies, very high Newtonian resistances should be assumed in the peripheral airways to produce frequency dependences consistent with Mead's model (19).

Peripheral inhomogeneity vs. input homogeneity. The results of simulation showed that, despite marked differences in the regional mechanical properties, the simulated ZL data can be fitted by models containing a

one-compartment periphery, with fitting errors not exceeding the low F values obtained in the actual measurements. In other words, the systematic errors, which are small even at elevated Zpaw, may remain hidden beyond fluctuations in the measured ZL data, and thus the peripheral inhomogeneity is not reflected by the input impedance of the lungs. This behavior appears in a striking analogy with the observation of interregional differences in the rate of change of P_{A_i}, inapparent in the maximum expiratory flow-volume curves (18). Nevertheless, we should stress here that our results relate to linear operation of the lung, both by the nature of the simulation model and because of the use of small-amplitude oscillations in the measurements.

If the lungs were characterized by a homogeneous one-compartment periphery or, alternatively, if the P_{A_i} data had been collected from peripheral branches corresponding to the mean $1/Zpaw_i$ of the distribution, the Ztr_i data could have been analyzed in terms of *model 1* or *2* parameters, and we could have seen whether the model-predicted separation of ZL into Zaw and Zti is congruent with the assumptions that all frequency-independent (Newtonian) resistances reside within the airway compartment and the tissue inertance comprises a minor portion of the total pulmonary inertance. Unfortunately, in view of the patterns of Ztr_i and Zaw_i, which were strikingly incompatible with those expected from a one-compartment periphery or a medium-impedance peripheral pathway, such an analysis would have led to uninterpretable results. We conclude that these patterns arise from the mutual shunt effects that the member impedances of the peripheral distribution exert on each other, particularly on those having relatively high values.

We have applied a simulation model that represents a largely simplified structure of the lungs, especially in view of the fact that an irregularly branching network was substituted here by a one-generation peripheral airways system. Consequently, neither the type nor the width of distribution of the peripheral parameters can be expected to correspond to real inhomogeneities. From a functional point of view, it may be nevertheless instructive that the $1/Zpaw_i$ values had to be distributed in a wide range (from 15.6 to 311.1% of the average value) to obtain in the highest-impedance branch such characteristic Ztr_i and Zaw_i curves as those found among the measured impedances (cf. data from *dogs 3* and *6* in Figs. 2 and 3 with Figs. 8 and 9 for Ztr_i and Fig. 7 with Fig. 9 for Zaw_i). Because it is unlikely that it was the highest-impedance branch we found quite often in capsules located on the large flat costal surfaces, the distribution of $Zpaw_i$ must have been substantially wider than that assumed in the simulation model. This is particularly relevant to the bronchoconstricted state, where two opposing effects on the inhomogeneity of P_{A_i} should be considered: the nonuniform responses to bronchoconstrictor stimuli may widen the distribution of $Zpaw_i$, whereas the marked increase of Zti acts in the direction of homogeneity of P_{A_i}. Consequently, if we had not kept Zti constant during the elevation of Zpaw, the ability to simulate the high-$Zpaw_i$ patterns would have required further widening of the distribution.

The maintenance of the initial distribution of $Zpaw_i$ during the elevation of Zpaw can be argued on the basis of the different local sensitivities to HI. Although the latter phenomenon is very likely to occur, in all except *dog 4* the pathways addressed by the capsule measurement seemed to preserve their positions in the distribution approximately; for example, the Rtr_i curves that ran farthest from the corresponding RL in control (i.e., that represented the highest-$Rpaw_i$ branch) did the same during HI (Fig. 2). This suggests that the irregular structure determining the initial inhomogeneity remained the dominant factor after the induced bronchoconstriction.

An interesting conclusion drawn from the simulations is that the effect of regional differences in the parenchymal mechanical properties is negligible not only on ZL but, in contrast with that in the peripheral airways, also on the local Ztr_i and Zaw_i data. This indicates that the interconnections through the $Zpaw_i$ network can create the functional homogeneity of the tissue units, even if we neglect the elastic coupling between them. On the other hand, the dissipative losses arising from the interregional flows may add to Rti (23), as was indicated by the virtual increase in B during the simulated elevation of Rpaw (Table 2). This phenomenon was interpreted on the basis of the interrupter resistance measurements by Bates et al. (2), in terms of a gas redistribution accompanying the stress recovery in the tissues. Increases in tissue resistance or viscance in excess of those in elastance have been observed during vagal stimulation (14), histamine inhalation (14, 15), and histamine infusion (present study), and these changes can be expressed by the elevation of η (8). However, because the contribution of interregional flows to the observed elevation in Rti could not be separated from the changes in the purely tissue resistance in any of these studies, the possible alterations in the intrinsic relationship between the dissipative and elastic properties at the elementary tissue level are really not known. In view of the limitations inherent in the present simulation study, it is only probable that the marked increase in η during HI (39 vs. the 18% elevation produced by the simulated bronchoconstriction) was due in part to a changed hysteresivity of the pulmonary tissue.

The authors thank I. Kopasz and L. Vigh for the excellent technical assistance.

This work was supported by Hungarian National Scientific Research Foundation Grant (OTKA 1074), the MTA-Soros Foundation, and National Heart, Lung, and Blood Institute Grant HL-33009.

Address for reprint requests: Z. Hantos, Kalmár Laboratory, József Attila University, PO Box 652, H-6701 Szeged, Hungary.

Received 7 May 1991; accepted in final form 30 August 1991.

REFERENCES

1. ALLEN, J. L., I. D. FRANTZ III, AND J. J. FREDBERG. Regional alveolar pressure during periodic flow: dual manifestations of gas inertia. *J. Clin. Invest.* 76: 620–629, 1985.
2. BATES, J. H. T., M. S. LUDWIG, P. D. SLY, K. BROWN, J. G. MARTIN, AND J. J. FREDBERG. Interrupter resistance elucidated by alveolar pressure measurement in open-chest normal dogs. *J. Appl. Physiol.* 65: 408–414, 1988.
3. BRUSASCO, V., D. O. WARNER, K. C. BECK, J. R. RODARTE, AND K. REHDER. Partitioning of pulmonary resistance in dogs: effect of tidal volume and frequency. *J. Appl. Physiol.* 66: 1190–1196, 1989.
4. DARÓCZY, B., A. FABULA, AND Z. HANTOS. Use of noninteger-mul-

tiple pseudorandom excitation to minimize nonlinear effects on impedance estimation. *Eur. Respir. Rev.* 1: 183–187, 1991.
5. DARÓCZY, B., AND Z. HANTOS. Generation of optimum pseudorandom signals for respiratory impedance measurements. *Int. J. Biomed. Comput.* 25: 21–31, 1990.
6. FREDBERG, J. J., R. H. INGRAM, JR., R. G. CASTILE, G. M. GLASS, AND J. M. DRAZEN. Nonhomogeneity of lung response to inhaled histamine assessed with alveolar capsules. *J. Appl. Physiol.* 58: 1914–1922, 1985.
7. FREDBERG, J. J., D. H. KEEFE, G. M. GLASS, R. G. CASTILE, AND I. D. FRANTZ III. Alveolar pressure nonhomogeneity during small-amplitude high-frequency oscillation. *J. Appl. Physiol.* 57: 788–800, 1984.
8. FREDBERG, J. J., AND D. STAMENOVIĆ. On the imperfect elasticity of lung tissue. *J. Appl. Physiol.* 67: 2408–2419, 1989.
9. HANTOS, Z., B. DARÓCZY, T. CSENDES, B. SUKI, AND S. NAGY. Modeling of low-frequency pulmonary impedance in dogs. *J. Appl. Physiol.* 68: 849–860, 1990.
10. HANTOS, Z., B. DARÓCZY, B. SUKI, G. GALGÓCZY, AND T. CSENDES. Forced oscillatory impedance of the respiratory system at low frequencies. *J. Appl. Physiol.* 60: 123–132, 1986.
11. HANTOS, Z., B. DARÓCZY, B. SUKI, AND S. NAGY. Low-frequency respiratory mechanical impedance in the rat. *J. Appl. Physiol.* 63: 36–43, 1987.
12. HANTOS, Z., B. SUKI, T. CSENDES, AND B. DARÓCZY. Constant-phase modelling of pulmonary tissue impedance (Abstract). *Bull. Eur. Physiopathol. Respir.* 23, *Suppl.* 12: 326s, 1987.
13. HILDEBRANDT, J. Comparison of mathematical models for cat lung and viscoelastic balloon derived by Laplace transform methods from pressure-volume data. *Bull. Math. Biophys.* 31: 651–667, 1969.
14. LORING, S. H., J. M. DRAZEN, J. C. SMITH, AND F. G. HOPPIN, JR. Vagal stimulation and aerosol histamine increase hysteresis of lung recoil. *J. Appl. Physiol.* 51: 477–484, 1981.
15. LUDWIG, M. S., I. DRESHAJ, J. SOLWAY, A. MUNOZ, AND R. H. INGRAM, JR. Partitioning of pulmonary resistance during constriction in the dog: effects of volume history. *J. Appl. Physiol.* 62: 807–815, 1987.
16. LUDWIG, M. S., J. J. MCNAMARA, R. G. CASTILE, G. M. GLASS, J. J. FREDBERG, AND R. H. INGRAM, JR. Lung inflation does not increase maximal expiratory flow during induced obstruction in the dog. *J. Appl. Physiol.* 65: 415–421, 1988.
17. LUDWIG, M. S., F. M. ROBATTO, P. D. SLY, M. BROWMAN, J. H. T. BATES, AND P. V. ROMERO. Histamine-induced constriction of canine peripheral lung: an airway or tissue response? *J. Appl. Physiol.* 71: 287–293, 1991.
18. MCNAMARA, J. J., R. G. CASTILE, G. M. GLASS, AND J. J. FREDBERG. Heterogeneous lung emptying during forced expiration. *J. Appl. Physiol.* 63: 1648–1657, 1987.
19. MEAD, J. Contribution of compliance of airways to frequency-dependent behavior of lungs. *J. Appl. Physiol.* 26: 670–673, 1969.
20. SLY, P. D., AND C. J. LANTERI. Differential responses of the airways and pulmonary tissues to inhaled histamine in young dogs. *J. Appl. Physiol.* 68: 1562–1567, 1990.
21. TOPULOS, G. P., G. J. NIELAN, G. M. GLASS, AND J. J. FREDBERG. Interdependence of regional expiratory flows limits alveolar pressure differences. *J. Appl. Physiol.* 69: 1413–1418, 1990.
22. VETTERMANN, J., D. O. WARNER, J.-F. BRICHANT, AND K. REHDER. Halothane decreases both tissue and airway resistances in excised canine lungs. *J. Appl. Physiol.* 66: 2698–2703, 1989.
23. WARNER, D. O. Alveolar pressure inhomogeneity during low-frequency oscillation of excised canine lobes. *J. Appl. Physiol.* 69: 155–161, 1990.
24. WARNER, D. O., R. E. HYATT, AND K. REHDER. Inhomogeneity during deflation of excised canine lungs. I. Alveolar pressures. *J. Appl. Physiol.* 65: 1757–1765, 1988.